Correction published 10 September 2004

Modeling estimates of the global emission of dimethylsulfide under enhanced greenhouse conditions

A. J. Gabric,[1] R. Simó,[2] R. A. Cropp,[1] A. C. Hirst,[3] and J. Dachs[4]

Received 4 November 2003; revised 11 March 2004; accepted 14 April 2004; published 5 June 2004.

[1] We have used a marine food-web model, an atmosphere-ocean general circulation model (GCM), and an empirical dimethylsulfide (DMS) algorithm to predict the DMS seawater concentration and the DMS sea-to-air flux in 10° latitude bands from 70°N to 70°S under contemporary and enhanced greenhouse conditions. The DMS empirical algorithm utilizes the food-web model predictions of surface chlorophyll and the GCM's simulation of oceanic mixed layer depth. The food-web model was first calibrated to contemporary climate conditions using satellite-derived chlorophyll data and meteorological forcings. For the climate change simulations, the meteorological forcings were derived from a transient simulation of the CSIRO Mark 2 GCM, using the IPCC/IS92a radiative forcing scenario to the period of equivalent CO_2 tripling (2080). The globally integrated DMS flux perturbation is predicted to be +14%; however, we found strong latitudinal variation in the perturbation. The greatest perturbation to DMS flux is simulated at high latitudes in both hemispheres, with little change predicted in the tropics and sub-tropics. The largest change in annual integrated flux (+106%) is simulated in the Southern Hemisphere between 50°S and 60°S. At this latitude, the DMS flux perturbation is most influenced by the GCM-simulated changes in the mixed layer depth. The results indicate that future increases in stratification in the polar oceans will play a critical role in the DMS cycle and climate change. *INDEX TERMS:* 0315 Atmospheric Composition and Structure: Biosphere/atmosphere interactions; 0312 Atmospheric Composition and Structure: Air/sea constituent fluxes (3339, 4504); 1615 Global Change: Biogeochemical processes (4805); 3210 Mathematical Geophysics: Modeling; *KEYWORDS:* climate change, dimethylsulfide (DMS), model

Citation: Gabric, A. J., R. Simó, R. A. Cropp, A. C. Hirst, and J. Dachs (2004), Modeling estimates of the global emission of dimethylsulfide under enhanced greenhouse conditions, *Global Biogeochem. Cycles*, *18*, GB2014, doi:10.1029/2003GB002183.

1. Introduction

[2] Climate change induced by human industrial activities is likely to perturb the planet's oceanic ecosystems [*Falkowski et al.*, 1998]; however, a quantitative assessment of the derived impact on the Earth system, though necessary, is an extremely difficult task. One of the characteristics of the functioning of the Earth system that hampers reliable projections of the planet's response to anthropogenic forcing is biogeochemical feedback, which may either reduce or amplify the net impact of the forcing [*Lovelock*, 1972]. One possible ecosystem feedback involves the marine planktonic food web and the biogenic sulfur compound dimethylsulfide (DMS), derived from its precursor compound dimethylsulfoniopropionate (DMSP), which is synthesized in phytoplankton cells and ubiquitous in the global ocean.

[3] DMS is the main, volatile sulfur species emanating from the oceans and therefore plays a major role in the atmospheric sulfur cycle [*Bates et al.*, 1992]. First *Shaw* [1983], and then *Charlson et al.* [1987], postulated a link between DMS, atmospheric sulfate aerosols, and global climate. It was hypothesized that global warming of the oceans would produce an increase in biogenically produced sulfate aerosol leading to formation of more cloud condensation nuclei (CCN), and brighter clouds, thus cooling the Earth's surface, and stabilizing climate against perturbations due to enhanced greenhouse gas emissions. This proposition, later called the CLAW hypothesis after the authors of the Charlson et al. paper, has stimulated a large research effort. Several large-scale studies inspired by the International Global Atmospheric Chemistry program (IGAC) have addressed aspects of the DMS-aerosol-climate connection, including ASTEX/MAGE [*Huebert et al.*, 1996], ACE-1 [*Bates et al.*, 1998], and AOE-91, 96 [*Leck et al.*, 1996]. Notwithstanding the publication of well over 1000 scientific papers on DMS in the past decade, and significant progress in the field, the original CLAW hypothesis still awaits a quantitative confirmation at the global scale.

[4] Early attempts to assess the direction and magnitude of the DMS-climate feedback [*Foley et al.*, 1991; *Lawrence*,

[1]Faculty of Environmental Sciences, Griffith University, Nathan, Queensland, Australia.
[2]Institut de Ciències del Mar (CMIMA-CSIC), Barcelona, Spain.
[3]CSIRO Atmospheric Research, Mordialloc, Victoria, Australia.
[4]Institut d'Investigacions Químiques i Ambientals (CID-CSIC), Barcelona, Spain.

0886-6236/04/2003GB002183

1993; *Gabric et al.*, 1998, 2001] indicated a small-to-moderate negative feedback on greenhouse gas radiative forcing (thus stabilizing climate), with magnitude of order 10–30%, and considerable regional variability. More recent studies in the Eastern Antarctic Southern Ocean predict a significant increase (+25%) in the DMS flux under warming [*Gabric et al.*, 2003]. Interestingly, the increase in flux was not due to higher in situ DMS production but mainly because of a loss of ice cover during summer-autumn and consequent increase in sea-to-air ventilation of DMS.

[5] One of the largest challenges in confirming or refuting the CLAW hypothesis is obtaining a complete understanding of the biological and biogeochemical processes that lead to net DMS production from DMSP and its emission to the atmosphere. The more we learn about it, the more complex the DMS cycle is revealed to be, which constrains our ability to address the CLAW hypothesis through truly mechanistic, quantitative modeling. DMSP is thought to act as an osmolyte and cryoprotectant in the algal cell, however its exact physiological role is still uncertain [*Stefels*, 2000]. The production of DMS from DMSP and its cycling in the upper ocean are directly linked to the dynamics of the marine planktonic food-web. The impact of warming on the food-web structure will affect DMS production, but the magnitude and direction of this change at the global scale is still unclear. It is significant that the climatically important variable, the DMS sea-to-air flux, seems to be a minor sink (less than 10%) in the overall cycle of DMS under current climatic conditions [*Wolfe et al.*, 1991; *Malin*, 1997; *Gabric et al.*, 1999], although this may change under an enhanced greenhouse climate.

[6] Improved understanding of the controls on DMS production has come from Lagrangian field studies, ocean time series, and use of large-scale mesocosms [*Kwint et al.*, 1996; *Turner et al.*, 1996; *Sakka et al.*, 1997; *Dacey et al.*, 1998]. The pathways of DMSP biosynthesis in phytoplankton have been studied and have shed light on potential regulating mechanisms such as nitrogen nutrition [*Grone and Kirst*, 1992; *Gage et al.*, 1997; *Keller et al.*, 1999], temperature [*Baumann et al.*, 1994], and light [*Vetter and Sharp*, 1993; *Matrai et al.*, 1995]. Although DMSP, and sometimes DMS, is partly released directly by phytoplankton, zooplankton also play a major role by mediating release through grazing, or by selecting or avoiding DMSP-rich cells [*Dacey and Wakeham*, 1986; *Leck et al.*, 1990; *Wolfe et al.*, 1994; *Tang*, 2000].

[7] The biological turnover of DMSP in seawater has been measured at 3–130 nM d^{-1} in non-bloom waters [*Leck et al.*, 1990; *Kiene*, 1996b; *Ledyard and Dacey*, 1996] with even higher rates being observed in blooms of DMSP-producing phytoplankton [*van Duyl et al.*, 1998]. The potential for DMS production is therefore quite large, but recent studies indicate that most of the DMSP in the sea is not converted to DMS. A demethylation/demethiolation pathway leading to production of methanethiol (MeSH) can account for 70–95% of DMSP metabolism in situ, thereby diverting sulfur away from DMS [*Kiene*, 1996a]. This process acts as a major biogeochemical control on DMS formation. The predominance of the non-DMS producing demethylation/demethiolation pathway may be explained by the fact that bacteria use it to assimilate the sulfur from DMSP into protein amino acids [*Kiene et al.*, 2000].

[8] Removal of DMS from the water column by biological [*Kiene and Bates*, 1990; *Leck et al.*, 1990] and photochemical [*Kieber et al.*, 1996; *Brugger et al.*, 1998] mechanisms also determine the net accumulation of DMS in surface waters. Biological consumption is an important sink for DMS under pseudo steady-state conditions, but appears to be slow to respond to rapid increases in DMS production [*Wolfe and Kiene*, 1993]. This may partially explain the rise in DMS concentrations observed at the peak and senescent phases of phytoplankton blooms [*Nguyen et al.*, 1988; *Matrai and Keller*, 1993]. Net consumption of DMS appears to occur in the later stages of blooms after DMS-consuming bacteria have had time to develop [*Kwint et al.*, 1996; *van Duyl et al.*, 1998]. The photochemical oxidation of DMS in seawater has been identified as a major removal mechanism under some circumstances [*Kieber et al.*, 1996] and appears to depend on the presence of photosensitizers in seawater, which are most likely part of the colored dissolved organic matter (CDOM).

[9] The DMS cycle underscores the intrinsic complexity of the marine planktonic system. For example, although there are now over 21,000 individual measurements of DMS throughout the world's oceans, attempts to correlate observed DMS concentrations with other commonly measured biological parameters, such as chlorophyll *a* or nutrients, have remained elusive [*Kettle et al.*, 1999]. Recently, however, *Simó and Dachs* [2002] reported a simple empirical relationship that permits global-ocean monthly distributions of DMS concentration to be computed from a combination of in situ or remotely sensed surface chlorophyll *a* and climatological data on the ocean mixed layer depth.

[10] Climate models all predict the planet's mean temperature will increase under the "business as usual" scenario [*Houghton et al.*, 1996]. Recent estimates of average equilibrium warming for a doubling of CO_2 are in the range 3.3 ± 0.8°K [*Grassl*, 2000]. However, there is strong spatial variation in this perturbation, with large sea surface temperature and salinity changes predicted to occur in the polar oceans [*Hirst*, 1999]. This warming and salinity reduction is generally accompanied by a shoaling of the oceanic mixed layer, and stronger illumination of the water column, which can affect both food-web dynamics and DMS production [*Gabric et al.*, 2001]. Under such conditions, photo-effects on the DMS pool become more important. Recently, *Sunda et al.* [2002] found that oxidative stressors, such as UV radiation, substantially increased cellular DMSP and its lysis into DMS in algal cultures. This confirms the suggestion made by *Simó and Pedrós-Alió* [1999] and *Kiene and Linn* [2000] that the yield of DMS from DMSP increases due to exposure to high solar irradiance.

[11] Recent model evaluations of the impact of climate change on regional DMS production in the Subantarctic and Antarctic Southern Oceans [*Gabric et al.*, 1998, 2001, 2003] point to strong regional variability in the DMS flux perturbation response (5–25%) and underscore the necessity for a global assessment of the DMS feedback. *Bopp et al.* [2003] recently gave a global assess-

ment of the change in DMS flux under warming. Under doubled equivalent CO_2, and therefore not directly comparable to the present work, their model estimated a small increase of global DMS flux to the atmosphere (+2%), but with large spatial heterogeneities (from −15% to +30% for the zonal mean).

[12] Here we assess the impact of simulated climate change on the production of DMS and give a quantitative assessment of one of the predictions of the CLAW hypothesis (that global warming would induce higher emissions of oceanic DMS) at a global scale. We have employed an existing food-web model to predict contemporary and future phytoplankton biomass as chlorophyll *a* (CHL) in 10° latitude zones from 70°N to 70°S. The CSIRO Mark 2 GCM was used to simulate the change in relevant forcings, including the mixed layer depth (MLD), under enhanced greenhouse conditions, up to the period corresponding to an equivalent tripling of pre-industrial atmospheric CO_2. In a departure from our previous modeling studies, where the DMS seawater concentration was predicted by one of the differential equations in the model [e.g., *Gabric et al.*, 1993], we have elected to use the empirical approach of *Simó and Dachs* [2002], (hereinafter called the SD algorithm), to predict the seawater DMS concentration.

2. Methods

2.1. DMS Empirical Algorithm

[13] Calibrating a multi-parameter process model such as that of *Gabric et al.* [1993] on a global grid would be a difficult task due to the very limited data on the spatial variability of the sulfur-specific rate constants. A more tractable approach for global DMS studies is provided by the SD algorithm, which was derived by using a combination of the *Kettle et al.* [1999] DMS database with concurrent CHL concentrations and climatological mixed layer depths. *Simó and Dachs* [2002] used regression analysis to derive a double-equation algorithm that allows prediction of monthly global surface DMS concentrations at any location in the ocean,

$$\mathrm{DMS} = (-1.0 \pm 0.3)\mathrm{Ln}(\mathrm{MLD}) + (5.7 \pm 1.0) \qquad \mathrm{CHL}/\mathrm{MLD} < 0.02 \tag{1a}$$

$$\mathrm{DMS} = (55.8 \pm 10.8)(\mathrm{CHL}/\mathrm{MLD}) + (0.6 \pm 0.9) \qquad \mathrm{CHL}/\mathrm{MLD} \geq 0.02. \tag{1b}$$

The units of DMS concentration are (nM), CHL (mg m^{-3}) with MLD measured in meters. Equations (1a) and (1b) were derived from analysis of monthly global distributions of CHL from the Sea-viewing Wide Field-of-View Sensor (SeaWiFS) and a global climatology of mean monthly MLD. The predicted DMS fields reproduce fairly well the major known patterns of global DMS variability, such as seasonal north-south shifts with concentration maxima in summer, high amplitude in the summer/winter concentration ratio at high latitudes, and low seasonal variability at low latitudes. The SD algorithm did not arise from chance, but a number of mechanisms underlying the equations were suggested.

[14] An inverse relationship between DMS concentration and CHL is apparent in a variety of oligotrophic regions [*Simó and Pedrós-Alió*, 1999]. In more productive regions, however, high DMS levels generally accompany local high CHL levels. Consequently, high DMS concentrations occur not only associated with very high CHL concentrations, but also with moderate-low CHL concentrations in waters with shallow mixing. This is because shallow mixing (low MLD) favors blooms of DMSP-producing taxa, highly efficient DMS-producing food webs, and an array of photochemical and photobiological effects that all lead to DMS accumulation [*Kieber et al.*, 1996; *Dacey et al.*, 1998; *Simó*, 2001].

2.2. Food-Web Model

[15] One of the challenges in this study is defining a model complexity that is capable of reproducing the variability in phytoplankton dynamics from 70°N to 70°S and is also computationally efficient. The current generation of oceanic food web models is well typified by the model of *Fasham et al.* [1990]. The approach is to have a small number of aggregated compartments representing generic autotrophs (phytoplankton) and grazers (micro-zooplankton). These models have been successfully used in location-specific studies, [e.g., *Doney*, 1996]; however, extrapolation to global or basin scales is hampered by the lack of generality of derived model parameterizations and, in some cases (e.g., where micro-nutrients such as iron may limit growth), the model's inherent formulation. Previous attempts at simulating the annual cycle in global phytoplankton have included the model of *Bopp et al.* [2001] which simulates SeaWiFS CHL reasonably well, yet gives significant overestimates in high-nitrate-low-chlorophyll (HNLC) regions such as the equatorial Pacific.

[16] With these limitations in mind, we have chosen a simple food-web structure and elected to calibrate the model to SeaWiFS chlorophyll in 10° latitudinal bands in order to better capture regional variability. The food-web model has been employed previously [*Gabric et al.*, 1993, 1999] and the dynamics of the model were studied extensively by *Cropp and Gabric* [2002]. Notwithstanding its simple ecological structure, this model can reproduce a surprisingly broad range of food-web dynamics [*Cropp*, 2003]. We note that in this analysis, the food-web model and the GCM are de-coupled, although the full embedding of the biological model in the GCM is a longer-term aim.

[17] The nitrogen-based model used here includes three biotic state variables: generic phytoplankton (P), zooplankton (Z), and dissolved nitrate (N). Total mass, N_0, is conserved in the mixed layer; that is, detrital losses are assumed to be exactly balanced by re-injection of nutrients from below the pycnocline. The state variables are vertically averaged over the oceanic mixed layer, where the MLD can vary throughout the year as prescribed by the output from the GCM simulation. The food-web model includes five biological rate parameters, an available nutrient concentra-

Table 1. Calibrated Model Parameter Values as Function of Latitude Band[a]

Band	k_1	k_2	k_3	M_o	k_s	I_k	N_o
60°N–70°N	0.0034	0.0082	0.682	1.646	43.226	35.9	14.570
50°N–60°N	0.0034	0.0080	0.685	2.080	43.636	37.1	14.500
40°N–50°N	0.041	0.127	0.339	0.914	25.122	40.3	7.295
30°N–40°N	0.179	0.193	0.404	1.452	21.305	47.5	3.653
20°N–30°N	0.355	0.233	0.256	3.023	24.526	49.0	1.592
10°N–20°N	0.400	0.288	0.343	3.018	12.108	47.3	3.235
0°–10°N	0.292	0.338	0.285	2.512	23.229	45.2	3.676
0°–10°S	0.430	0.506	0.262	3.224	6.921	46.0	3.629
10°S–20°S	0.376	0.219	0.400	2.346	6.846	48.6	4.529
20°S–30°S	0.430	0.165	0.454	2.540	5.692	51.3	4.730
30°S–40°S	0.113	0.117	0.322	1.711	12.199	49.5	4.924
40°S–50°S	0.087	0.167	0.232	1.890	18.974	43.3	3.206
50°S–60°S	0.088	0.148	0.196	1.774	14.663	37.5	3.244
60°S–70°S	0.0708	0.117	0.199	1.724	10.197	35.0	3.500

[a]Notation: k_1, zooplankton grazing rate (d^{-1} (mgN $m^{-3})^{-1}$); k_2, zooplankton mortality rate (d^{-1}); k_3, zooplankton excretion (–); μ_o, phytoplankton maximum nitrate uptake rate (d^{-1}); k_s, half-saturation nitrate concentration (mgN m^{-3}); I_k, saturating irradiance (W m^{-2}); N_o, total nitrate concentration (mgN m^{-3}).

tion, and three parameters (see Table 1) describing the physical forcing on the phytoplankton growth rate,

$$\frac{dP}{dt} = \mu P - k_1 PZ, \tag{2a}$$

$$\frac{dZ}{dt} = k_1(1-k_3)PZ - k_2 Z, \tag{2b}$$

$$\frac{dN}{dt} = k_1 k_3 PZ + k_2 Z - \mu P, \tag{2c}$$

$$N_0 = P + Z + N. \tag{2d}$$

Phytoplankton nitrate-specific growth rate, μ in equation (2a), has been parameterized using the standard multiplicative form, with the growth contemporaneously limited by nutrient availability (R_N), light (R_L) and temperature (R_T),

$$\mu = \mu_0 R_N R_L R_T, \tag{3a}$$

$$R_N = \frac{N}{N + k_s}, \tag{3b}$$

$$R_L = \left(\frac{1}{I_k}\right) \Big/ \sqrt{1 + (I/I_k)^2}, \tag{3c}$$

$$R_T = e^{0.063(T - T_{\max})}, \tag{3d}$$

where each limitation coefficient is in the range, $0 < R_i < 1$. Here μ_o is the maximum phytoplankton growth rate, k_s is the nitrate half-saturation concentration, I is the mixed-layer mean irradiance (PAR), and I_k is the saturating irradiance [*Talling*, 1957]. Laboratory culture studies on various algal species show a clear temperature effect (equation (3d)) on the growth rate of phytoplankton [*Eppley*, 1972], with $T_{\max}$ the maximum annual mixed layer temperature. Meteorological forcings for the contemporary climate simulations were obtained from current global databases. The sea-surface temperature (SST) data was derived from the Pathfinder AVHRR data set covering the period (1985–1999). The PAR data was from the Sea-viewing Wide Field-of-View Sensor (SeaWiFS) [*Lewis*, 1995] 8-day archive (1997–2001). Wind speed data were from the QuickSCAT SeaWinds, (1999–2001) archive. Mixed layer depths are from the Levitus World Ocean Atlas [*Boyer and Levitus*, 1994]. Monthly mean ice-cover data was derived from the Special Sensor Microwave Imager (SSMI) archive for the period (1992–2001).

[18] The food-web model was calibrated to satellite-derived CHL, which was zonally averaged in 10° latitude bands. The time series of CHL concentrations was derived from 3 years of SeaWiFS (8-day) Standard Mapped Images. Cloud is a major problem for satellite measurement of ocean color, especially at high latitudes, and consequently the percentage of pixels that contained chlorophyll data varied latitudinally. Ranges for each of the model parameters were estimated from the literature, and the food-web model was calibrated using the mean annual cycle in satellite-derived algal biomass. Forcing data for the contemporary climate calibration were obtained from existing databases and satellite data. Parametric estimation for the calibration was done using a genetic algorithm (GA) which is an efficient, non-derivative based optimization technique that mimics natural evolution [*Holland*, 1975]. GAs initially randomly sample the search space, and evaluate the "fitness" of each point according to a defined fitness or goal function. GAs build up a picture of the "fitness landscape," and search for optimum solutions by sampling near points of high fitness.

[19] Least squares estimators (equation (4)) are commonly used as goal functions when fitting deterministic models to time series data (y_i, t_i) [*Fasham and Evans*, 1995],

$$L.S.E. = \sum_{i=1}^{N} (y_i - y(t_i, \boldsymbol{k}))^2, \tag{4}$$

where, $y(t_i, \boldsymbol{k})$ is the model predicted value, which is a function of the parameter vector $\boldsymbol{k}$. [*Press et al.*, 1992] suggest minimizing a chi-square statistic (equation (5)) if the standard deviations of the data points are not constant.

$$\chi^2 = \sum_{i=1}^{N} \left(\frac{y_i - y(t_i, \boldsymbol{k})}{\sigma_i}\right)^2. \tag{5}$$

This statistic allows an estimate of the statistical significance of the fit. *Press et al.* [1992] note that large standard deviations σ_i associated with the data points y_i can lead to misinterpretation of the statistical significance of the goodness-of-fit. The satellite data sets have high variance (coefficients of variation of 16–88%) due to the effects of cloud and the large area of the zones, suggesting that a χ^2 statistic may be misleading. Consequently, both a least squares and a χ^2 estimator were implemented, and compared, as measures of fitness. Each point in the seven-dimensional parameter space visited by the GA was used to integrate the food-web model for sufficient time to reach a

repeating annual cycle. The fitness was calculated from the goodness of fit.

[20] The GA was first configured to undertake an extensive search of the parameter space, so that an appreciation of the sensitivity of the estimators to the various parameters could be obtained. The GA was implemented with a population of 30 individuals evolving for 50 generations, using initial and final mutation and crossover probabilities of 0.01–0.005 and 0.75–0.975, respectively. The probabilities were varied during the simulation according to a power law. The reproductive success of individuals was implemented using sigma-scaled Monte Carlo selection to prevent premature convergence of the GA [*Mitchell*, 1996]. Scaling reduced the probability of reproductive success of an individual with fitness two standard deviations above the mean from up to 50 times that of an individual 2 standard deviations below the mean, to 3 times. Each estimator was implemented 10 times by the GA. The coefficients of variation of the mean parameter values of the optimum parameter set found in each implementation were used as indicators of the sensitivity of the estimators to each of the parameters.

2.3. CSIRO Mark 2 CGCM

[21] The transient climate data was obtained from simulations with the Commonwealth Scientific and Industrial Research Organization (CSIRO) Mark 2 coupled climate model which includes ocean, atmosphere and sea-ice components [*Gordon and O'Farrell*, 1997]. The horizontal resolution of the atmospheric model is 5.6° of longitude by 3.2° of latitude (strictly, it is a spectral model of R21 resolution), and it has nine vertical levels. The sea-ice model was described by *O'Farrell* [1997]. The ocean model is based on the Bryan-Cox code [*Cox*, 1984] with 21 vertical levels. Further details of the ocean component are given by *Gordon and O'Farrell* [1997] and *Hirst et al.* [2000].

[22] The coupled GCM was initialized using the final spin-up state of the atmosphere-ocean system, which resulted from several thousand years of integration. The control integration used a constant equivalent CO_2 concentration of 330 ppm and was used to evaluate the statistical significance of trends predicted in the transient integration. The transient integration is subject to changing equivalent CO_2 concentration as specified in the IPCC/ISP92a radiative forcing scenario following the prescription of *Kattenberg et al.* [1996] for the period from 1880 to 2086 (for details about this run and its evaluation, see *Hirst* [1999]). A subset of the output from GCM simulations for the two periods 1961–1970 (baseline), and 2078–2086 (tripled equivalent CO_2) was obtained for the entire globe between 70°N and 70°S. The relevant forcing data for the food-web model was zonally averaged in 10° bands and included sea-surface temperature, wind speed at the surface, cloud cover, sea-ice cover, and MLD.

2.4. Sea-to-Air Flux Parameterization

[23] As DMS is highly supersaturated in the surface ocean, the sea-to-air flux of DMS is computed as the product of the sea-to-air DMS transfer velocity k_w and the sea-water DMS concentration, $[DMS]_{aq}$,

$$F_{DMS} = k_w[DMS]_{aq}. \quad (6)$$

The transfer velocity was parameterized in terms of wind speed, w, and sea surface temperature according to the piece-wise linear formulation of *Liss and Merlivat* [1986], as adapted for DMS by *Gabric et al.* [1995, 1996],

$$k_w = \alpha 0.17w \qquad w \le 3.6, \quad (7a)$$

$$k_w = \beta(2.85w - 10.3) + 0.61\alpha \qquad 3.6 < w \le 13, \quad (7b)$$

$$k_w = \beta(5.9w - 49.9) + 0.61\alpha \qquad w > 13, \quad (7c)$$

with $\alpha = (600/\mathrm{Sc})^{2/3}$ and $\beta = (600/\mathrm{Sc})^{1/2}$. For a given gas, the Schmidt number (Sc) varies with water temperature, decreasing as the temperature increases. The dependence of *Sc* on sea surface temperature (T) for DMS was experimentally derived by *Saltzman et al.* [1993] as

$$Sc = 2674.0 - 147.12(T) + 3.726(T)^2 - 0.038(T)^3. \quad (8)$$

[24] We note that empirical gas exchange-wind speed relationships have to be applied with caution, since they have an uncertainty of up to a factor of 2. Although other formulations of the sea-to-air DMS flux exist [e.g., *Wanninkhof and McGillis*, 1999], the *Liss and Merlivat* [1986] parameterization used here has provided excellent estimates of DMS flux in the Subantarctic Southern Ocean [*Ayers et al.*, 1995]. The calculation of k_w in seasonal ice zones poses special difficulties since DMS release from sea-ice during melting or break-up is well documented, and ice algae have also been shown to be significant producers of DMS and DMSP in the polar oceans [*Kirst et al.*, 1991; *Levasseur et al.*, 1994]. We assume that DMS ventilation can only occur in ice-free waters. This implies that our estimates of flux are likely to be a lower bound on the true flux. It also means that the simulated change in flux will be affected by ice-cover changes. In this analysis, the computed DMS transfer velocity was scaled by the percentage of ice-free water as predicted by the GCM.

3. Results and Discussion

3.1. Calibration of Food-Web Model to SeaWiFS Chlorophyll

[25] The zonal mean forcings for SST, PAR and MLD used in the calibration of the CHL prediction are shown in Figures 1–3. Results of the model parameter calibration against the SeaWiFS phytoplankton data are given in Table 1, with the best-fit annual cycle in CHL shown in Figure 4. Bearing in mind our simplified food-web representation, the model fit to the mean satellite chlorophyll data is very good. The model captures the dynamics particularly well at high latitudes; however, the weak seasonal signal in CHL in the tropics and subtropics meant the GA had difficulty in assigning an unambiguous parameter set in these regions. However, the calibration did not have problems reproducing the general magnitude of the CHL cycle

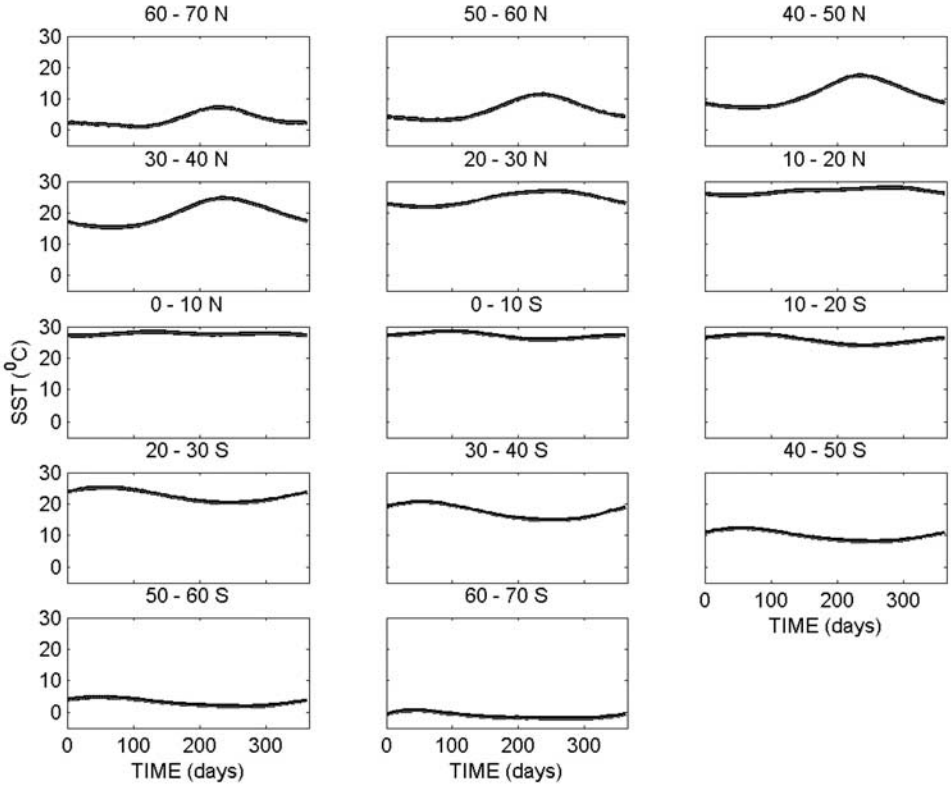

Figure 1. Zonal mean contemporary sea surface temperature.

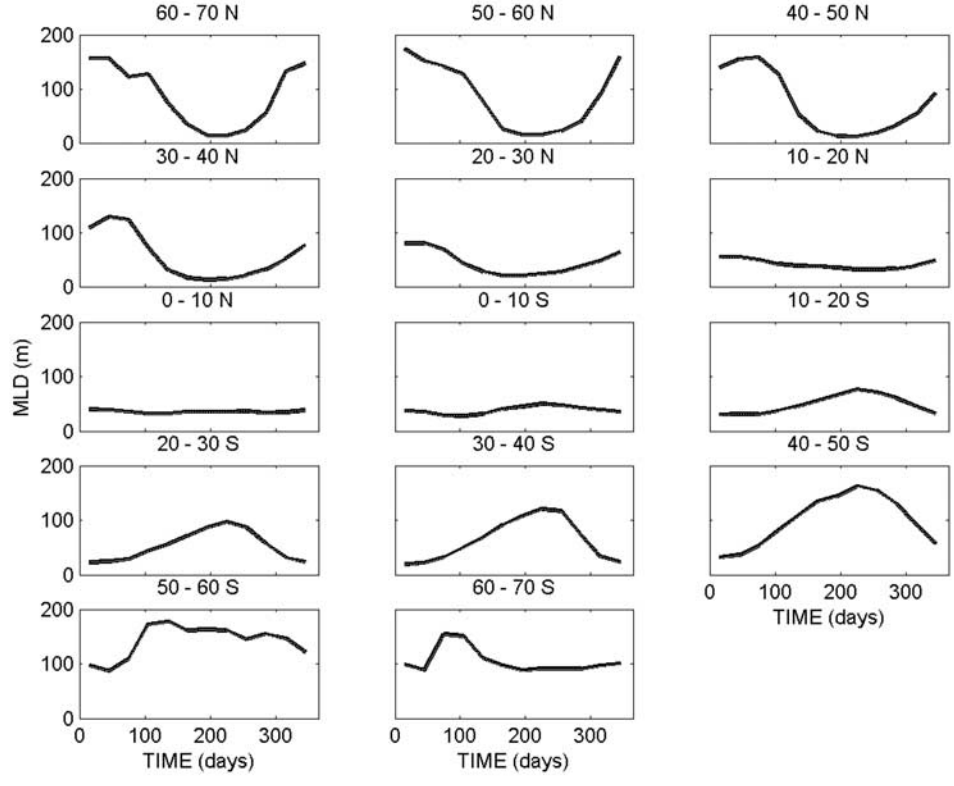

Figure 2. Zonal mean MLD from Levitus data set.

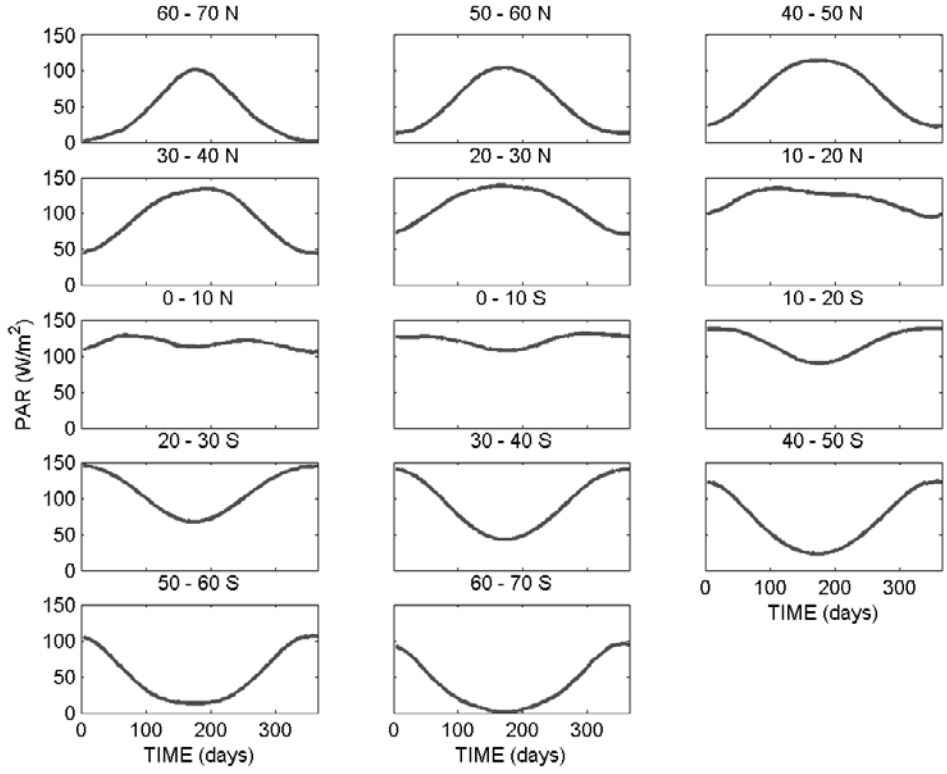

Figure 3. Zonal mean SeaWiFS photosynthetically available radiation.

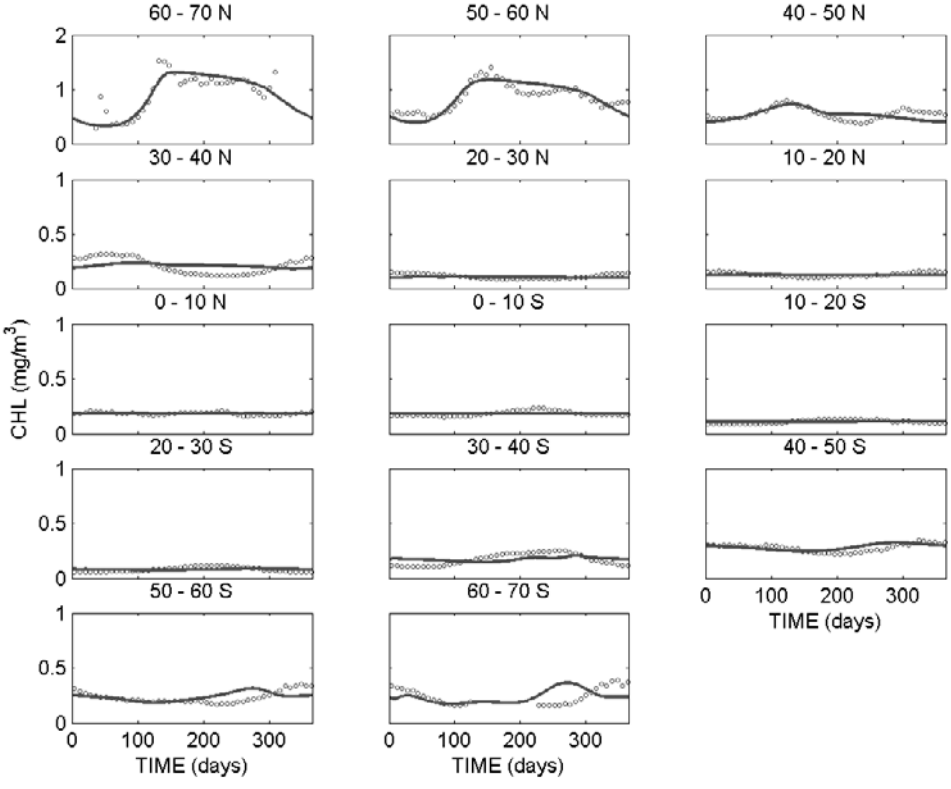

Figure 4. Contemporary zonal mean SeaWiFS chlorophyll (open circles) and fitted model chlorophyll prediction (solid line). Note that data are not available throughout the entire year at high latitudes.

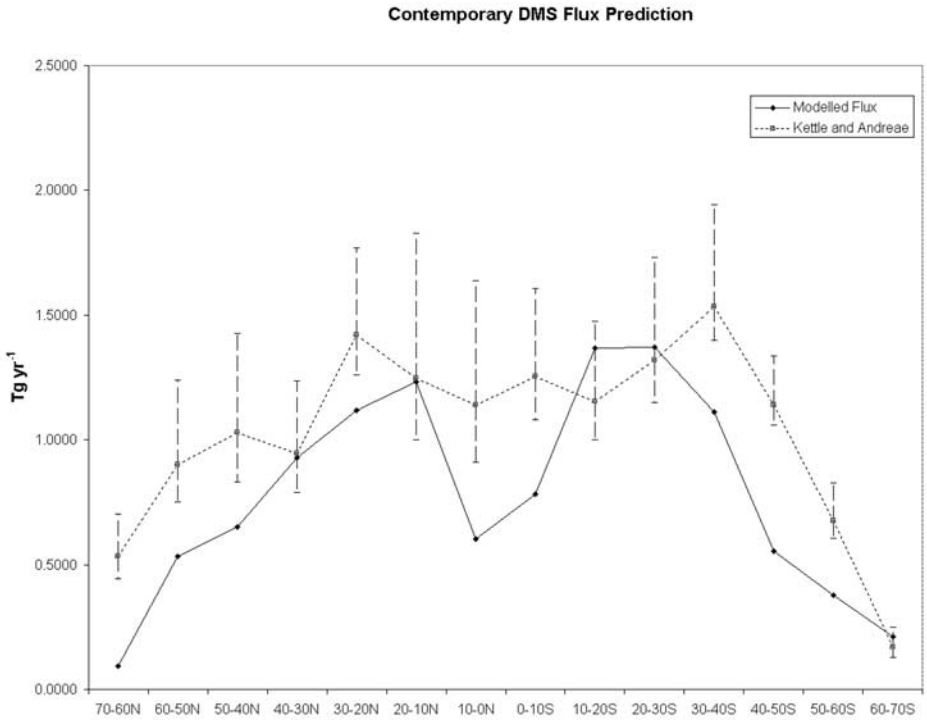

Figure 5. Contemporary annual integrated DMS flux prediction by latitude band modeled compared with Kettle database.

in the subtropical gyres. The general trend in the parameter values with latitude is consistent with our understanding of global phytoplankton distribution patterns. For example, k_1 (zooplankton grazing rate) and μo (phytoplankton maximum growth rate) show a steady increase from the poles to the equator. It should be noted that N_o (the total mixed layer nitrate concentration) is best interpreted as a measure of the amount of nutrient assimilated in the food web. The latitudinal trend in this parameter reflects the high nutrient demands in the Arctic and Subarctic regions and the low demand in the subtropical gyres. The relatively low N_o value in the Southern Ocean reflects the low assimilation of nutrients in this region.

[26] The contemporary zonal CHL predictions were then combined with the SD algorithm and the wind, temperature, and MLD climatologies to generate a DMS flux prediction in each latitude band. In order to evaluate our approach, we have compared the modeled contemporary flux with the mean of the four global DMS flux estimates presented by *Kettle and Andreae* [2000] for the same transfer velocity formulation of *Liss and Merlivat* [1986] used here. The flux results are shown in Figure 5 and compare reasonably well with the data, albeit slightly underestimating the flux at high latitudes. The annual total DMS flux (70°N–70°S) is predicted to be 11 Tg yr^{-1} compared with the mean estimate of *Kettle and Andreae* [2000] of 14.4 Tg yr^{-1}.

3.2. GCM Simulations of Forcings

[27] The GCM simulated change (3 × CO_2 value – baseline value) in the relevant meteorological forcings under enhanced greenhouse conditions are shown in Figures 6–10. We note that in the SD algorithmequations (1a) and (1b), the DMS concentration has an inverse dependence on MLD. However, the MLD will also affect the CHL value predicted by the food-web model. This "dual dependence" suggests the DMS flux perturbation will be sensitively dependent on the GCM's simulation of the change in MLD.

[28] The GCM simulated change in zonal mean SST (Figure 6) shows a general warming across our study region in the range 1°–4°K, with a more pronounced response in the Northern Hemisphere relative to the Southern Hemisphere. The largest change (+4.1°K) is in the 50°N–60°N band, during late summer. The simulated change in zonal mean wind speed (Figure 7) is small for most of the study region, with a slight increase during the summer months in both hemispheres. The GCM simulates a slight increase in winter sea ice in both polar regions; however, there is a largest simulated decrease in sea-ice cover in the Arctic Ocean at high latitudes (>70°N) during late summer and autumn, outside our study region. The GCM simulated change in cloud cover is generally small (<10%) throughout the study region. Of particular significance for the DMS cycle is the large simulated decrease in MLD (Figure 8) throughout the year in the Southern Ocean (50°S–70°S), with the maximum change during spring and early summer. The proportional change in MLD is in the range 20–40%. Such a large decrease in MLD is not simulated in the Northern Hemisphere.

3.3. Simulated Change in DMS Flux

[29] Model predictions for the change in monthly DMS flux as a function of zonal band are shown in Figure 9,

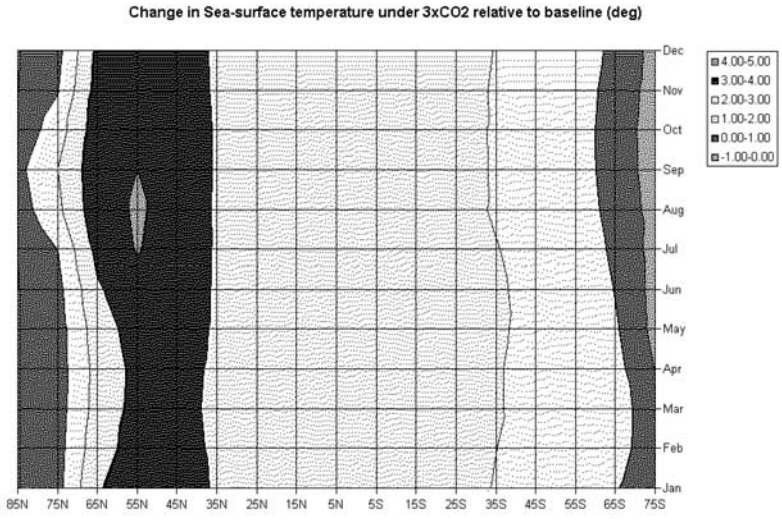

Figure 6. GCM simulated change in monthly mean zonal sea-surface temperature as a function of latitude. See color version of this figure at back of this issue.

and the annual integrated flux perturbation is given in Table 2. The total global flux perturbation between 70°N and 70°S is predicted to be +14.2%; however as shown in Table 2, there is considerable regional variability in the DMS flux response. Significant increases in DMS flux are confined to high latitudes during spring and early summer. The Southern Hemisphere experiences the largest increases south of 40°S, while the Northern Hemisphere experiences significant increases only north of 50°N.

[30] In order to better understand the reasons for DMS flux change, we examine the predictions more closely in the 50°S–60°S band, where the largest relative flux perturbations are simulated. At 50°S–60°S, the mean monthly DMS flux (Figure 10a) is predicted to increase under enhanced greenhouse conditions by factor between 11 in spring to 1.3 in late summer. In this region, the ratio (CHL/MLD) is <0.02 for both contemporary and enhanced greenhouse conditions due to relatively deep MLDs (Figure 10b), thus the first part (equation (1a)) of the SD algorithm applies, and the predicted DMS seawater concentration is independent of CHL and reflects the seasonal change in MLD. The simulated annual cycles in k_w is shown in Figure 10c. The transfer velocity increases only slightly during the autumn-winter period, due to the small change in wind speed simulated by the GCM in this band (Figure 7).

[31] Although not used as a predictor of DMS at this latitude, it is still notable that the food-web model predicts a general increase in biomass throughout the

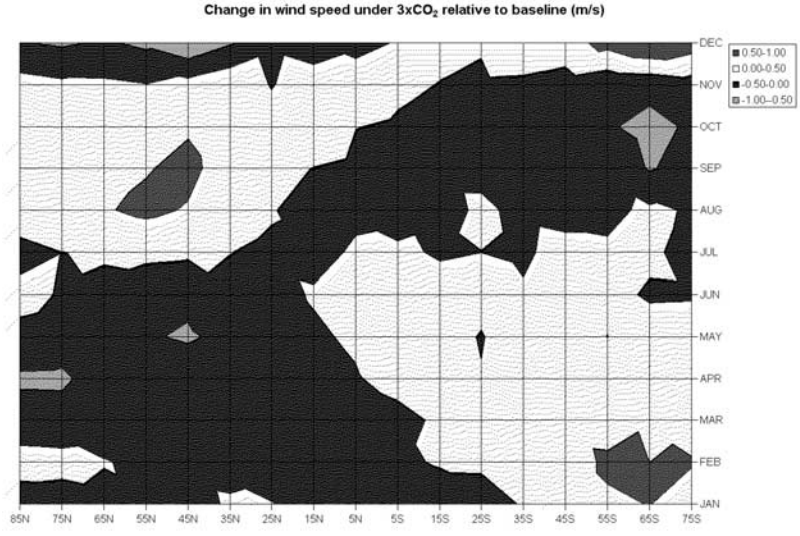

Figure 7. GCM simulated change in monthly mean zonal wind speed at sea surface as a function of latitude. See color version of this figure at back of this issue.

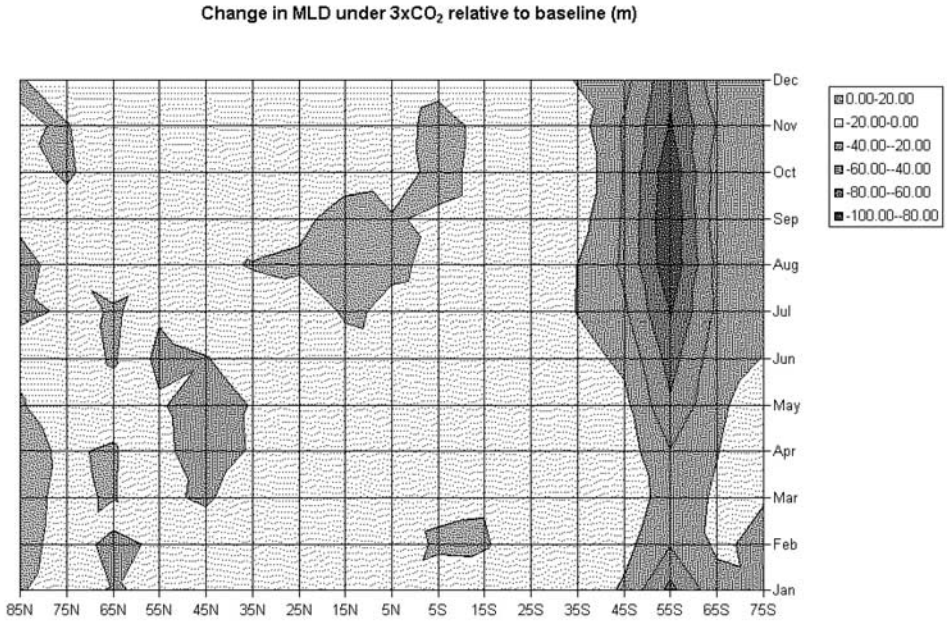

Figure 8. GCM simulated change in mean monthly MLD as a function of latitude. See color version of this figure at back of this issue.

year (Figure 10d), with a longer phytoplankton growth season in summer and autumn. Importantly for phytoplankton growth, the MLD falls to below 100 m for most of the summer period, thus partly relieving light limitation, which is a key factor controlling phytoplankton growth at high southern latitudes [*Boyd*, 2002]. In summary, the predicted DMS flux increase at high southern latitudes is mainly attributable to the slight increase in k_w, the slight decrease in sea-ice, and the significant shallowing of the MLD simulated by the GCM.

[32] By comparison, the situation at 50°N–60°N (not shown) is quite different from the Southern Ocean, in that the (CHL/MLD) ratio exceeds 0.02 during spring and summer, so that both CHL and MLD are influential in predicting the DMS concentration (equation (1b)). Although there is a general shoaling of the MLD under warming, the

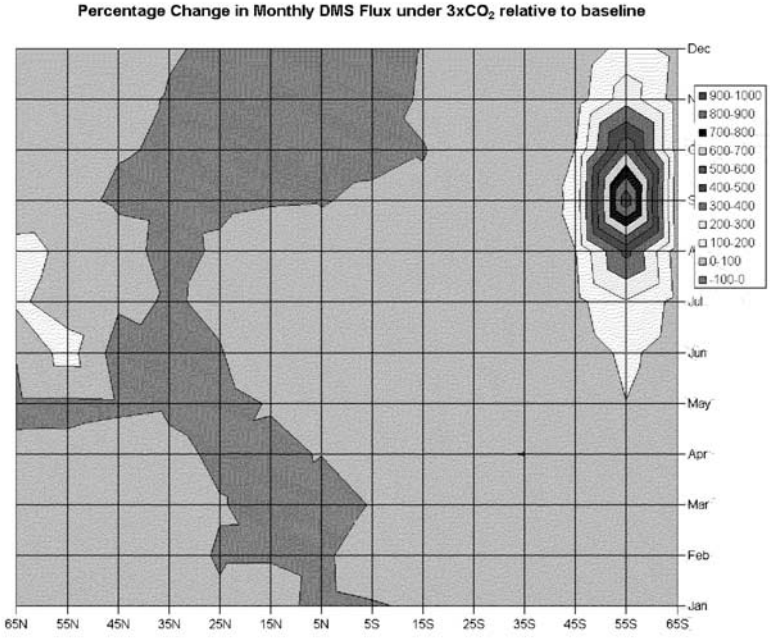

Figure 9. Predicted change in zonal mean monthly DMS flux as a function of latitude. See color version of this figure at back of this issue.

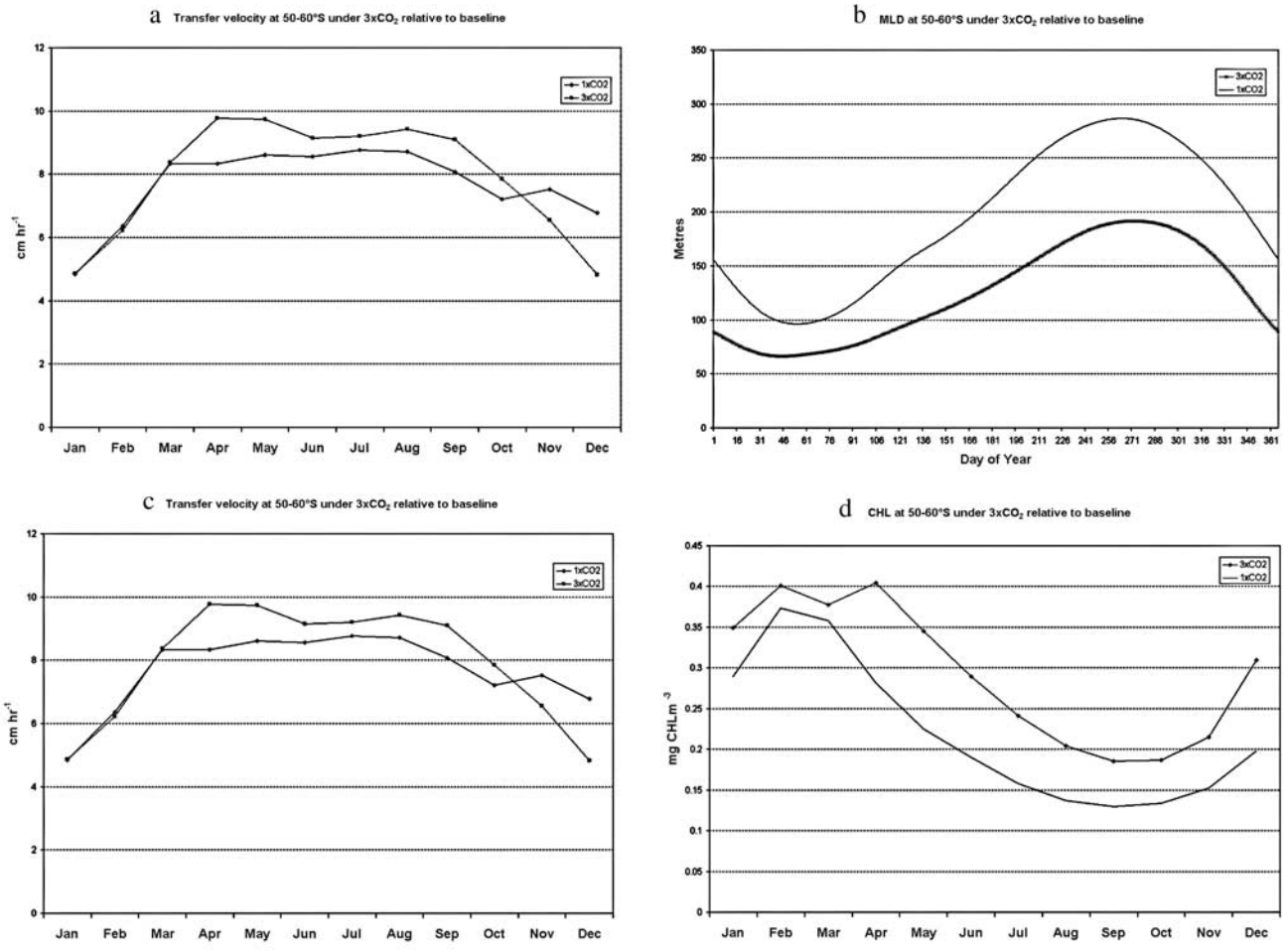

Figure 10. The changes at 50°S–60°S in (a) DMS flux, (b) MLD (c) transfer velocity, k_w, and (d) biomass, [CHL].

MLD under both contemporary and enhanced greenhouse conditions is less than 100 m for most of the year, so that light limitation is not critical for phytoplankton growth. Phytoplankton biomass does increase slightly during spring under warming, with the peak in biomass occurring earlier in the year, due to a shift in the phenology of the bloom. However, a general increase in CHL is not evident. As a consequence, the predicted seasonal cycles in DMS and MLD are not as closely coupled as they are in the Southern Ocean.

[33] The only other work that has attempted a global DMS flux perturbation analysis is that of *Bopp et al.* [2003], who considered the impact of doubling equivalent CO_2. These authors noted a similar general trend to that found here. They found strong latitudinal variability in the zonal mean flux change, with major increases in subtropics and high latitudes of both hemispheres (up to 19%), consistent with our findings (allowing for the difference in climate forcing scenarios), but a stronger decrease in the equatorial ocean (−15%) compared with our result.

3.4. Consequences for Radiative Forcing

[34] The chemical and physical pathways that lead from atmospheric DMS to sulfur particles are complex and still poorly understood. There have been a number of recent papers debating the role of DMS in new particle formation in the marine boundary layer and raising the possibility that sea salt and other large particles act as an effective sink for DMS, limiting its ability to generate CCN [*Pirjola et al.*, 2000; *Yoon and Brimblecombe*, 2002]. However, the strong

Table 2. Perturbation in Zonally-Averaged Annual DMS Flux by Latitude Band

Band	Change in Annual DMS Flux %	Change in DMS Ventilated, Tg S yr^{-1}
70°N–60°N	19.5	0.0038
60°N–50°N	28.9	0.0279
50°N–40°N	−2.2	−0.0052
40°N–30°N	2.2	0.0058
30°N–20°N	−3.6	−0.0135
20°N–10°N	5.5	0.0307
10°N–0°	−7.2	−0.0156
0°–10°S	3.7	0.0101
10°S–20°S	5.9	0.0323
20°S–30°S	6.5	0.0385
30°S–40°S	10.7	0.0698
40°S–50°S	32.3	0.1814
50°S–60°S	106.9	0.2610
60S°–70°S	46.3	0.0476

seasonal coherence in signals of DMS, CCN, and MSA recorded in clean marine atmospheres [*Ayers and Gras*, 1991] provides strong evidence for a DMS-derived source, at least in remote, unpolluted regions.

[35] The climatic consequences of the increase DMS flux at middle to high latitudes could be quite significant. Although a quantitative estimate of the climate feedback awaits a full ''online'' coupling of the climate and biogeochemical models, it is possible that cloud microphysical changes in these regions resulting from the strong DMS-derived aerosol changes could have a significant effect on subpolar and polar radiation budgets. This would be most significant in spring/summer, which in turn could have an effect on snow/ice melt rates, and could possibly induce an ice/albedo feedback amplification of the initial signal.

[36] Following the analysis of *Gabric et al.* [1998], we assume an empirical relation between DMS flux and CCN concentration at high southern and northern latitudes similar to that measured at the Cape Grim (Tasmania) location in the Subantarctic. Thus a mean enhancement of +14% in DMS flux and a mean summer flux of 5 μmole m^{-2} d^{-1} would lead to of radiative forcing due to DMS derived aerosols of (-0.75 ± 0.2) Wm^{-2} (combined direct and indirect forcings). By way of comparison, the climate model simulations suggest that a tripling of equivalent CO_2 concentration contributes an increase in longwave radiative forcing of the troposphere of $\sim$+6.9 Wm^{-2} consistent with other climate model simulations [*Houghton et al.*, 1996]. Thus the mean DMS flux perturbation in this polar region represents a negative feedback strength of about 11%. Clearly, our results show the DMS response to warming will vary regionally and the extrapolation to a global scale is thus problematic. An improved evaluation of the feedback will only be possible with an embedding of the DMS model in the GCM, which is planned for the near future.

4. Conclusions

[37] We have presented a modeling analysis of the global DMS response to simulate climate change. A food-web model was used to predict mixed layer chlorophyll and an empirical algorithm was employed to predict the DMS concentration under contemporary and GCM simulated enhanced greenhouse conditions. The zonal mean DMS flux perturbation was computed in 10° latitude bands from 70°N to 70°S. The strong regional variability in the simulated DMS flux response, with little change in the tropics and major increases predicted at high latitudes, is a significant result, and emphasizes the importance of gaining a better understanding of the polar marine biomes and their response to future climate change.

[38] There are several sources of uncertainty we would point out about this analysis. We have assumed that the marine food web gradually adapts to warming and that no significant species distribution changes will occur. However, contemporary ecological data indicate that planktonic populations can respond extremely sensitively and quickly to ocean variability. Long-term climate-plankton connections have been detected in the Pacific in the CalCOFI programme [e.g., *Roemmich and McGowan*, 1995] and in the North Atlantic in the Continuous Plankton Recorder surveys [*Colebrook*, 1979]. We have also not explicitly included any changes to nutrient supply (either from modifications in upwelling or Aeolian deposition) to the surface ocean under warming, although we note that coupled climate models do predict that upwelling will be reduced, especially in the tropics, as the oceans warm [e.g., *Bopp et al.*, 2001]. As the tropical regions are not predicted to experience large increases in DMS flux, this omission is unlikely to significantly affect our conclusions.

[39] Although warming has a noticeable impact on phytoplankton dynamics in the simulations, the perturbation to DMS flux obtained here is largely the result of simulated physical changes (a decrease in MLD) in the water column. However, we recognize that the net ventilation of DMS is the result of whole food-web interactions, with traits such as nonlinearity and multiple feedbacks that are typical of a complex system and difficult to predict. Our results should be reasonable if one accepts that in the short-term (<100 years), only shifts in the biogeography and timing of plankton communities are to be expected, rather than strong adaptations or major shifts in community structure. Gaining an improved understanding of the role of marine biota in climate is a formidable challenge, which will only be met by a coordinated mix of long-term observational and theoretical studies.

[40] **Acknowledgments.** The authors wish to thank the SeaWiFS Project (Code 970.2) and the Distributed Active Archive Centre (Code 902) at the Goddard Space Flight Center, Greenbelt, Maryland, for the production and distribution of the SeaWiFS data, respectively. These activities are sponsored by NASA's Mission to Planet Earth Program (http://seawifs.gsfc.nasa.gov). The Quikscat/SeaWinds and Advanced Very High Resolution Radiometer data were obtained from the NASA Physical Oceanography Distributed Active Archive Center at the Jet Propulsion Laboratory/California Institute of Technology (http://podaac.jpl.nasa.gov). The SSMI data was provided by the Defense Meteorological Satellite Program, National Oceanic and Atmospheric Administration, U.S. Department of Commerce (http://www.ncdc.noaa.gov). The NODC (Levitus) World Ocean Atlas 1994 data were provided by the NOAA-CIRES Climate Diagnostics Center, Boulder, Colorado (http://www.cdc.noaa.gov/). The World Ocean Atlas 1998 was supplied by the Ocean Climate Laboratory, National Oceanographic Data Center, National Oceanic and Atmospheric Administration, U.S. Department of Commerce (http://www.nodc.noaa.gov). We are grateful for the efforts of many members of the Climate Modelling and Applications Team that are responsible for the development of CSIRO climate models. Finally, we gratefully acknowledge the financial assistance of an ASAC Grant from the Australian Antarctic Division and an Australian Research Council Large Grant.

References

Ayers, G. P., and J. L. Gras (1991), Seasonal relationship between cloud condensation nuclei and aerosol methanosulphonate in marine air, *Nature*, *353*, 834–835.

Ayers, G. P., S. T. Bentley, J. P. Ivey, and B. W. Forgan (1995), Dimethylsulphide in marine air at Cape Grim, 41°S, *J. Geophys. Res.*, *100*(D10), 21,013–21,021.

Bates, T. S., B. K. Lamb, A. Guenther, J. Dignon, and R. E. Stoiber (1992), Sulfur emissions to the atmosphere from natural sources, *J. Atmos. Chem.*, *14*, 325–337.

Bates, T. S., B. J. Huebert, J. L. Gras, F. B. Griffiths, and P. A. Durkee (1998), International Global Atmospheric Chemistry (IGAC) Project's First Aerosol Characterization Experiment (ACE-1): Overview, *J. Geophys. Res.*, *103*(D13), 16,297–16,318.

Baumann, M. E. M., F. P. Brandini, and R. Staubes (1994), The influence of light and temperature on carbon-specific DMS release by cultures of Phaeocystis antarctica and three Antarctic diatoms, *Mar. Chem.*, *45*, 129–136.

Bopp, L., P. Monfray, O. Aumont, J. L. Dufresne, H. Le Treut, G. Madec, L. Terray, and J. C. Orr (2001), Potential impact of climate change on marine export production, *Global Biogeochem. Cycles*, *15*(1), 81–99.

Bopp, L., O. Aumont, S. Belviso, and P. Monfray (2003), Potential impact of climate change on marine dimethyl sulfide emissions, *Tellus, Ser. B*, *55*(1), 11–22.

Boyd, P. W. (2002), Environmental factors controlling phytoplankton processes in the Southern Ocean, *J. Phycol.*, *38*, 844–861.

Boyer, T. P., and S. Levitus (1994), Quality control and processing of historical temperature, salinity and oxygen data, *NOAA Tech. Rep. NESDIS 81*, 65 pp., Natl. Oceanic and Atmos. Admin., Silver Spring, Md.

Brugger, A., D. Slezak, I. Obernosterer, and G. J. Herndl (1998), Photolysis of dimethylsulfide in the northern Adriatic Sea: Dependence on substrate concentration, irradiance and DOC concentration, *Mar. Chem.*, *59*, 321–331.

Charlson, R. J., J. E. Lovelock, M. O. Andreae, and S. G. Warren (1987), Oceanic phytoplankton, atmospheric sulphur, cloud albedo and climate, *Nature*, *326*, 655–661.

Colebrook, J. M. (1979), Continuous plankton records: Seasonal cycles of phytoplankton and copepods in the North Atlantic Ocean and the North Sea, *Mar. Biol.*, *51*, 23–32.

Cox, M. D. (1984), A primitive equation, 3-dimensional model of the ocean, *GFDL Ocean Group Tech. Rep. 1*, 141 pp., Geophys. Fluid Dyn. Lab., Princeton Univ., Princeton, N. J.

Cropp, R. (2003), A biogeochemical modelling analysis of the potential for marine ecosystems to regulate climate by the production of dimethylsulphide, Ph.D. thesis, 283 pp., Griffith Univ., Nathan, Queensland, Australia.

Cropp, R., and A. J. Gabric (2002), Ecosystem adaptation: Do ecosystems maximise resilience?, *Ecology*, *83*(7), 2019–2026.

Dacey, J. W. H., and S. G. Wakeham (1986), Oceanic dimethylsulfide: Production during zooplankton grazing on phytoplankton, *Science*, *233*, 1314–1316.

Dacey, J. W. H., F. A. Howse, A. F. Michaels, and S. G. Wakeham (1998), Temporal variability of dimethylsulfide and dimethylsulfoniopropionate in the Sargasso Sea, *Deep Sea Res., Part I*, *45*, 2085–2104.

Doney, S. C. (1996), A synoptic atmospheric surface forcing data set an physical upper ocean model for the U.S. JGOFS Bermuda Atlantic Time-Series Study site, *J. Geophys. Res.*, *101*(C11), 25,615–25,634.

Eppley, R. W. (1972), Temperature and phytoplankton growth in the sea, *Fish. Bull.*, *70*, 1063–1085.

Falkowski, P. G., R. T. Barber, and V. Smetacek (1998), Biogeochemical controls and feedbacks on ocean primary production, *Science*, *281*, 200–206.

Fasham, M. J. R., and G. T. Evans (1995), The use of optimization techniques to model marine ecosystem dynamics at the JGOFS station at 47°N 20°W, *Philos. Trans. R. Soc. London, Ser. B*, *348*, 203–209.

Fasham, M. J. R., H. W. Ducklow, and S. M. McKelvie (1990), A nitrogen-based model of plankton dynamics in the oceanic mixed layer, *J. Mar. Res.*, *48*, 591–639.

Foley, J. A., K. E. Taylor, and S. J. Ghan (1991), Planktonic dimethylsulfide and cloud albedo: An estimate of the feedback response, *Clim. Change*, *18*, 1–15.

Gabric, A. J., C. N. Murray, L. Stone, and M. Kohl (1993), Modeling the production of dimethylsulphide during a phytoplankton bloom, *J. Geophys. Res.*, *98*(C12), 22,805–22,816.

Gabric, A. J., G. P. Ayers, and G. C. Sander (1995), Independent marine and atmospheric model estimates of the sea-air flux of dimethylsulfide in the Southern Ocean, *Geophys. Res. Lett.*, *22*(24), 3521–3524.

Gabric, A. J., G. P. Ayers, C. N. Murray, and J. Parslow (1996), Use of remote sensing and mathematical modelling to predict the flux of dimethylsulphide to the atmosphere in the Southern Ocean, *Adv. Space Res.*, *18*(7), 117–128.

Gabric, A. J., P. Whetton, R. Boers, and G. P. Ayers (1998), The impact of GCM predicted climate change on the air-to-sea flux of dimethylsulphide in the subantarctic Southern Ocean, *Tellus, Ser. B*, *50*, 388–399.

Gabric, A. J., P. Matrai, and M. Vernet (1999), Modelling the production of dimethylsulphide during the vernal bloom in the Barents Sea, *Tellus, Ser. B*, *51*, 919–938.

Gabric, A. J., P. Whetton, and R. Cropp (2001), Dimethylsulphide production in the subantarctic Southern Ocean under enhanced greenhouse conditions, *Tellus, Ser. B*, *53*, 273–287.

Gabric, A. J., R. Cropp, A. Hirst, and H. Marchant (2003), The sensitivity of dimethylsulphide production to simulated climate change in the eastern Antarctic Southern Ocean, *Tellus, Ser. B*, *55*, 966–981.

Gage, D. A., D. Rhodes, K. D. Nolte, W. A. Hicks, T. Leustek, A. J. L. Cooper, and A. D. Hanson (1997), A new route for synthesis of dimethylsulfoniopropionate in marine algae, *Nature*, *387*, 891–893.

Gordon, H. G., and S. P. O'Farrell (1997), Transient climate change in the CSIRO coupled model with dynamic sea ice, *Mon. Weather Rev.*, *125*, 875–907.

Grassl, H. (2000), Status and improvements of coupled general circulation models, *Science*, *288*, 1991–1997.

Grone, T., and G. O. Kirst (1992), The effect of nitrogen deficiency, methionine, and inhibitors of methionine metabolism on the DMSP contents of Tetraselmis subcordiformes (Stein), *Mar. Biol.*, *112*, 497–503.

Hirst, A. C. (1999), The Southern Ocean response to global warming in the CSIRO coupled ocean atmosphere model: Special issue on Global Change, *Environ. Model. Software*, *14*, 227–241.

Hirst, A. C., S. P. O'Farrell, and H. B. Gordon (2000), Comparison of a coupled ocean-atmosphere model with and without oceanic eddy-induced advection: I. Ocean spinup and control integrations, *J. Clim.*, *13*(1), 139–163.

Holland, J. H. (1975), *Adaptation in Natural and Artificial Systems*, Univ. of Mich. Press, Ann Arbor.

Houghton, J. T., L. G. Meira Filho, B. A. Callander, N. Harris, A. Kattenberg, and S. K. E. Varney (1996), *Climate Change 1995: Contribution of Working Group 1 to the Second Assessment Report of the IPCC*, 572 pp., Cambridge Univ. Press, New York.

Huebert, B. J., A. Pszenny, and B. Blomquist (1996), The ASTEX/MAGE experiment, *J. Geophys. Res.*, *101*(D2), 4319–4329.

Kattenberg, A., F. Giorgi, H. Grassl, G. A. Meehl, F. B. Mitchell, R. J. Stouffer, T. Tokioka, A. J. Weaver, and T. M. L. Wigley (1996), Climate models: Projections of future climate, in *Climate Change 1995: The Science of Climate Change*, edited by J. T. Houghton et al., pp. 285–357, Cambridge Univ. Press, New York.

Keller, M. D., R. Kiene, and P. A. Matrai (1999), Production of glycine betaine (GBT) and dimethylsulfonio propionate (DMSP) in nitrogen-limited chemostats cultures of marine phytoplankton, *Mar. Biol.*, *135*, 249–257.

Kettle, A. J., and M. O. Andreae (2000), Flux of dimethylsulphide from the oceans: A comparison of updates data sets and flux models, *J. Geophys. Res.*, *105*(D22), 26,793–26,808.

Kettle, A. J., M. O. Andreae, D. Amouroux, T. W. Andreae, T. S. Bates, H. Berresheim, and R. Boniforti (1999), A global database of sea surface dimethylsulfide (DMS) measurements and a procedure to predict sea surface DMS as a function of latitude, longitude and month, *Global Biogeochem. Cycles*, *13*(2), 399–444.

Kieber, D. J., J. F. Jiao, R. P. Kiene, and T. S. Bates (1996), Impact of dimethyl sulfide photochemistry on methyl sulphur cycling in the equatorial Pacific Ocean, *J. Geophys. Res.*, *101*(C2), 3715–3722.

Kiene, R. P. (1996a), Production of methane thiol from dimethylsulfoniopropionate in marine surface waters, *Mar. Chem.*, *54*, 69–83.

Kiene, R. P. (1996b), Turnover of dissolved DMSP in estuarine and shelf waters from the Northern Gulf of Mexico, in *Environmental and Biological Chemistry of DMSP and Related Sulfonium Compounds*, edited by R. Kiene et al., pp. 337–349, Plenum, New York.

Kiene, R. P., and T. S. Bates (1990), Biological removal of dimethylsulphide from seawater, *Nature*, *345*, 702–705.

Kiene, R. P., and L. J. Linn (2000), Distribution and turnover of dissolved DMSP and its relationship with bacterial production and dimethylsulfide in the Gulf of Mexico, *Limnol. Oceanogr.*, *45*, 849–861.

Kiene, R. P., L. J. Linn, and J. A. Bruton (2000), New and important roles for DMSP in marine microbial communities, *J. Sea Res.*, *43*, 209–224.

Kirst, G. O., C. Thiel, H. Wolff, J. Nothnagel, M. Wanzek, and U. R. (1991), Dimethylsulfoniopropionate (DMSP) in ice algae and its possible biological role, *Mar. Chem.*, *35*, 381–388.

Kwint, R. L. J., P. Quist, T. A. Hansen, L. Dijkhuizen, and K. J. M. Kramer (1996), Turnover of dimethylsulfoniopropionate and dimethylsulfide in the marine environment: A mesocosm experiment, *Mar. Ecol. Prog. Ser.*, *145*, 223–232.

Lawrence, M. G. (1993), An empirical analysis of the strength of the phytoplankton-dimethylsulfide-cloud-climate feedback cycle, *J. Geophys. Res.*, *98*(D11), 20,663–20,673.

Leck, C., U. Larsson, L. E. Bågander, S. Johansson, and S. Hajdu (1990), DMS in the Baltic Sea: Annual variability in relation to biological activity, *J. Geophys. Res.*, *95*(C3), 3353–3363.

Leck, C., E. K. Bigg, D. S. Covert, J. Heintzenberg, W. Maenhaut, E. D. Nilsson, and A. Wiedensohler (1996), Overview of the atmospheric research programme during the International Arctic Ocean Expedition of 1991 (IAOE-91) and its scientific results, *Tellus, Ser. B*, *48*, 136–155.

Ledyard, K. M., and J. W. H. Dacey (1996), Microbial cycling of DMSP and DMS in coastal and oligotrophic seawater, *Limnol. Oceanogr.*, *41*, 33–40.

Levasseur, M., M. Gosselin, and S. Michaud (1994), A new source of dimethyl sulfide for the Arctic atmosphere, *Mar. Biol.*, *121*, 381–387.

Lewis, M. R. (1995), Coastal Zone Color Scanner on Nimbus and Sea-Viewing Wide Field-of-View Sensor on Seastar, in *Oceanographic Applications of Remote Sensing*, edited by M. Ikeda and F. W. Dobson, pp. 167–181, CRC, Boca Raton, Fla.

Liss, P. S., and L. Merlivat (1986), Air-sea gas exchange rates: Introduction and synthesis, in *The Role of Air-Sea Exchange in Geochemical Cycling*, edited by P. Buat-Menard, pp. 113–127, D. Reidel, Norwell, Mass.

Lovelock, J. E. (1972), Gaia as seen through the atmosphere, *Atmos. Environ.*, *6*, 579–580.

Malin, G. (1997), Sulphur, climate and the microbial maze, *Nature*, *387*, 857–859.

Matrai, P. A., and M. D. Keller (1993), Dimethylsulfide in a large-scale coccolithophore bloom in the Gulf of Maine, *Cont. Shelf Res.*, *13*, 831–843.

Matrai, P. A., M. Vernet, R. Hood, A. Jennings, S. Saemundsdottir, and E. Brody (1995), Light-dependent production of DMS and carbon incorporation by polar strains of Phaeocystis spp., *Mar. Biol.*, *124*, 157–167.

Mitchell, M. (1996), *An Introduction to Genetic Algorithms*, MIT Press, Cambridge, Mass.

Nguyen, B. C., S. Belviso, N. Mihalopoulos, J. Gostan, and P. Nival (1988), Dimethylsulfide production during natural phytoplanktonic blooms, *Mar. Chem.*, *24*, 133–141.

O'Farrell, S. P. (1997), Investigation of the dynamic sea ice component of a coupled atmosphere-sea ice general circulation model, *J. Geophys. Res.*, *103*(C8), 15,751–15,782.

Pirjola, L., C. D. O'Dowd, I. M. Brooks, and M. Kulmala (2000), Can new particle formation occur in the clean marine boundary layer?, *J. Geophys. Res.*, *105*(D21), 26,531–26,546.

Press, W. H., S. A. Teukolsky, W. T. Vetterling, and B. P. Flannery (1992), *Numerical Recipes in FORTRAN: The Art of Scientific Computing*, Cambridge Univ. Press, New York.

Roemmich, D., and J. McGowan (1995), Climatic warming and the decline of zooplankton in the California current, *Science*, *256*, 1311–1313.

Sakka, A., M. Gosselin, M. Levasseur, S. Michaud, P. Montfort, and S. Demers (1997), Effects of reduced ultraviolet radiation on aqueous concentrations of dimethylsulfoniopropionate and dimethylsulfide during microcosm studies in the lower St. Lawrence Estuary, *Mar. Ecol. Prog. Ser.*, *149*, 227–238.

Saltzman, E. S., D. B. King, K. Holmen, and C. Leck (1993), Experimental determination of the diffusion coefficient of dimethylsulfide in water, *J. Geophys. Res.*, *98*(C9), 16,481–16,486.

Shaw, G. E. (1983), Bio-controlled thermostasis involving the sulphur cycle, *Clim. Change*, *5*, 297–303.

Simó, R. (2001), Production of atmospheric sulfur by oceanic plankton: Biogeochemical, ecological and evolutionary links, *Trends Ecol. Evol.*, *16*, 287–294.

Simó, R., and J. Dachs (2002), Global ocean emission of dimethylsulfide predicted from biogeophysical data, *Global Biogeochem. Cycles*, *16*(4), 1018, doi:10.1029/2001GB001829.

Simó, R., and C. Pedrós-Alió (1999), Role of vertical mixing in controlling the oceanic production of dimethylsulphide, *Nature*, *402*, 396–399.

Stefels, J. (2000), Physiological aspects of the production and conversion of DMSP in marine algae and higher plants, *J. Sea Res.*, *43*, 183–197.

Sunda, W., D. J. Kieber, R. P. Kiene, and S. Huntsman (2002), An antioxidant function for DMSP and DMS in marine algae, *Nature*, *418*, 317–320.

Talling, J. F. (1957), Photosynthetic characteristics of some freshwater plankton diatoms in relation to underwater radiation, *New Phytol.*, *56*, 29–50.

Tang, K. W. (2000), Dynamics of dimethylsulfoniopropionate (DMSP) in a migratory grazer: A laboratory simulation study, *J. Exp. Mar. Biol. Ecol.*, *243*, 283–293.

Turner, S. M., G. Malin, P. D. Nightingale, and P. S. Liss (1996), Seasonal variation of dimethylsulphide in the North Sea and an assessment of fluxes to the atmosphere, *Mar. Chem.*, *54*, 245–262.

van Duyl, F. C., W. W. C. Gieskes, A. J. Kop, and W. E. Lewis (1998), Biological control of short-term variation in the concentration of DMSP and DMS during a *Phaeocystis* spring bloom, *J. Sea Res.*, *40*, 221–231.

Vetter, Y., and J. H. Sharp (1993), The influence of light intensity on dimethylsulfide production by a marine diatom, *Limnol. Oceanogr.*, *38*, 419–425.

Wanninkhof, R., and W. R. McGillis (1999), A cubic relationship between air-sea CO_2 exchange and wind speed, *Geophys. Res. Lett.*, *26*(13), 1889–1892.

Wolfe, G. V., and R. P. Kiene (1993), Radioisotope and chemical inhibitor measurements of dimethyl sulfide consumption rates and kinetics in estuarine waters, *Mar. Ecol. Prog. Ser.*, *99*, 261–269.

Wolfe, G. V., T. S. Bates, and R. J. Charlson (1991), Climatic and environmental implications of biogas exchange at the sea's surface: Modeling DMS and the marine biologic cycle, in *Ocean Margin Processes in Global Change*, edited by R. F. C. Mantoura et al., 469 pp., John Wiley, New York.

Wolfe, G. V., E. B. Sherr, and B. F. Sherr (1994), Release and consumption of DMSP from Emiliana huxleyi during grazing by Oxyrrhis marina, *Mar. Ecol. Prog. Ser.*, *111*, 111–119.

Yoon, Y. J., and P. Brimblecombe (2002), Modelling the contribution of sea salt and dimethyl sulfide derived aerosol to marine CCN, *Atmos. Chem. Phys.*, *2*, 17–30.

R. A. Cropp and A. J. Gabric, Faculty of Environmental Sciences, Griffith University, Nathan, Qld, 4111 Australia. (a.gabric@griffith.edu.au)

J. Dachs, Institut d'Investigacions Químiques i Ambientals (CID-CSIC), Jordi Girona 18-22, 08034 Barcelona, Spain.

R. Simó, Institut de Ciències del Mar (CMIMA-CSIC), Pg Marítim de la Barceloneta 37-49, 08003 Barcelona, Spain.

A. C. Hirst, CSIRO Atmospheric Research, Private Bag 1, Mordialloc, Vic, 3185 Australia.

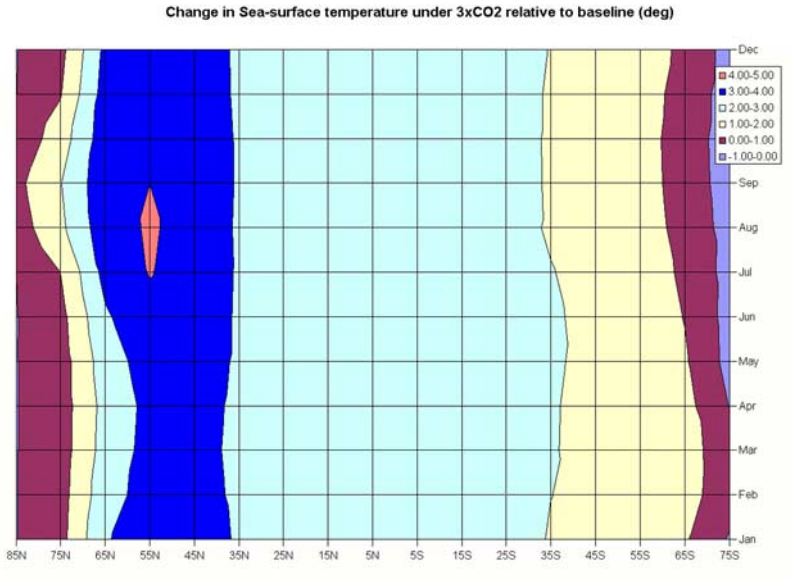

Figure 6. GCM simulated change in monthly mean zonal sea-surface temperature as a function of latitude.

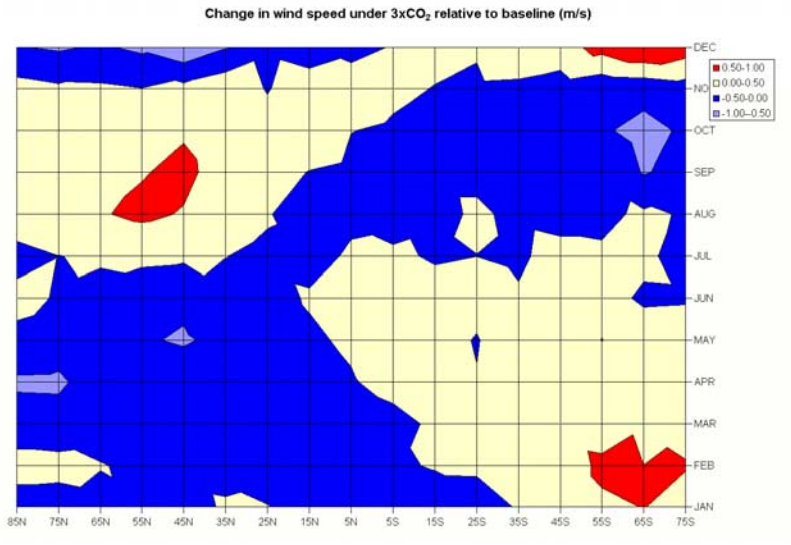

Figure 7. GCM simulated change in monthly mean zonal wind speed at sea surface as a function of latitude.

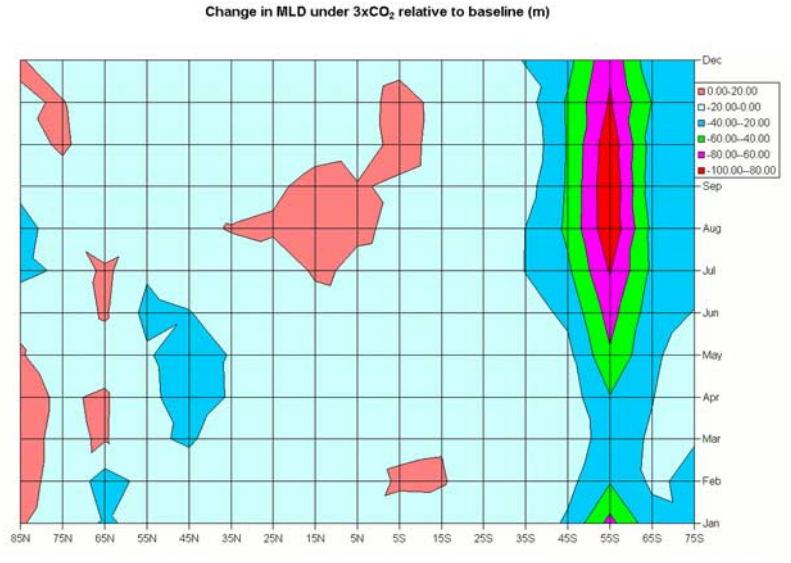

Figure 8. GCM simulated change in mean monthly MLD as a function of latitude.

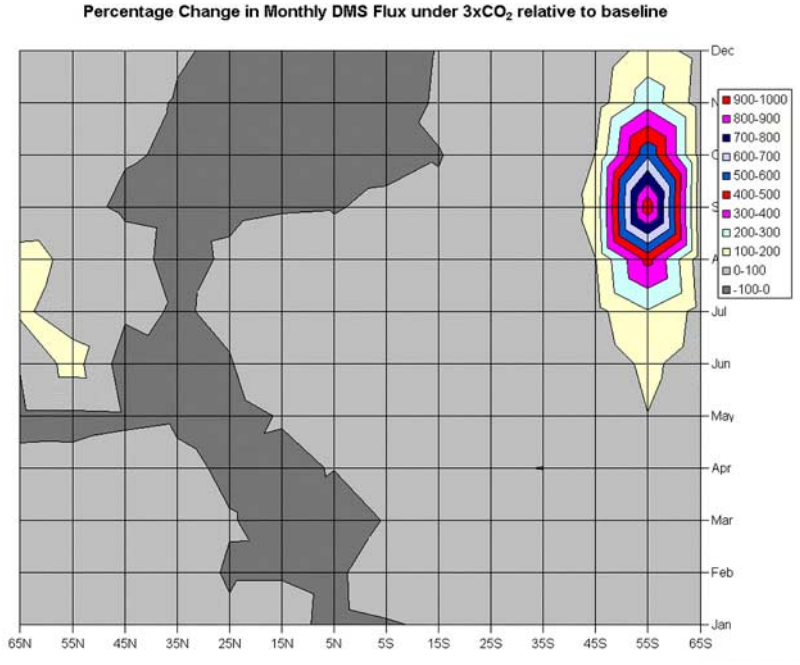

Figure 9. Predicted change in zonal mean monthly DMS flux as a function of latitude.